14th European Signal Processing Conference (EUSIPCO 2006), Florence, Italy, September 4-8, 2006, copyright by EURASIP

ATOMIC DECOMPOSITION BASED DETECTOR FOR DENOISING IN ISAR IMAGING

Omar A. Yeste Ojeda and Jesús Grajal

Universidad Politécnica de Madrid
Departamento de Señales, Sistemas y Radiocomunicaciones
Madrid, Spain

ABSTRACT

We have investigated two different strategies to improve the quality of ISAR images corrupted by Gaussian noise. The images are generated using a Time Frequency technique known as Atomic Decomposition (AD). The first strategy is a classical denoising technique based on an AD detector developed for signal detection in noise. The second technique separates the atoms extracted through AD by their parameters in two classes: atoms coming from noise and atoms coming from signal components. Compared to the first one, the second technique requires a greater knowledge about the signal components.

1. INTRODUCTION

Joint time-frequency analysis is a powerful tool with applications in signal analysis, detection and estimation [1]-[4]. It pursues the meaningful representation of signals in both the time and frequency domains in order to reveal their spectral behavior along the time.

Among the wide variety of time-frequency representations, Atomic Decomposition (AD) [5, 6], also known as Matching Pursuit [2, 7], Adaptive Gabor Representation [3] or Adaptive Chirplet Transform [8], has attracted considerable attention over the last decade, as it offers new possibilities in different areas related to radar.[1]

We have already explored the possibilities of AD in signal interception applications [11, 12], where sensitivity is crucial. It has been shown that AD presents better sensitivity than other approaches if an appropriate dictionary is used, e.g., the chirplet family when detecting chirped signals [11]. Moreover, AD also provides a meaningful representation of signals which becomes very useful for recognizing the signal modulation [11].

Apart from interception, there are other radar-related applications where AD is used. For instance, AD is used in SAR/ISAR imaging in order to obtain focused and denoised images, as well as for extracting target features [9, 10, 13, 14, 15]. In these applications the sensitivity is not the limiting requirement but the quality of the image and computational burden.

This paper analyses the characteristics of the AD-based ISAR images and the denoising capabilities offered by AD. The denoising of ISAR images is not a very common topic in the literature. Nevertheless, readers can found in [21] an interesting denoising algorithm based on basis pursuit [2], while our algorithm is based on a detection approach. Since that algorithm decomposes the signal as a sum of complex sinusoids, the observation time must be short in order to minimise blurring effects of acceleration. Decomposing the signal into chirplets allows longer coherent integration times, which is necessary to improve the sensitivity.

This work has been supported by the National Grant Program FPU and the project TIC-2002-04569-C02-01.

[1] In the radar literature, Atomic Decomposition has been termed in different manners, such as Adaptive Joint Time-Frequency Algorithm [9], Adaptive Wavelet Transform [10].

2. THE ATOMIC DECOMPOSITION TECHNIQUE

2.1 Theoretical Overview

The aim of AD is to represent the signal (vector) under analysis, $\mathbf{x}$, as the weighted sum of a set of elementary functions named atoms:

$$\mathbf{x} = \sum_p \widehat{b}_p \, \mathbf{h}_{\widehat{\gamma}_p} \, . \tag{1}$$

These atoms are estimated through an iterative procedure maximizing, at each iteration, the inner product of a residual signal and the atoms of the dictionary [3],[5]-[7]:

$$\widehat{\gamma}_p = \arg\max_{\gamma} \left| \mathbf{h}_{\gamma}^{\mathrm{H}} \, \mathbf{x}_{p-1} \right|^2 , \tag{2}$$

$$\widehat{b}_p = \mathbf{h}_{\gamma}^{\mathrm{H}} \, \mathbf{x}_{p-1} \, , \tag{3}$$

where the superscript H indicates complex conjugate transposition and $\mathbf{x}_p$ denotes the residual signal after the p-th iteration. This residual signal is updated for the next iteration by substracting its orthogonal projection onto the estimated atom:

$$\mathbf{x}_p = \begin{cases} \mathbf{x}_{p-1} - \widehat{b}_p \, \mathbf{h}_{\widehat{\gamma}_p} & p = 1, 2, \dots \, , \\ \mathbf{x} & p = 0 \, . \end{cases} \tag{4}$$

Due to the sequential character of the estimation of the atoms, AD is a greedy algorithm. As a result, AD can estimate more energetic atoms than any of the signal components when these components are close in the time-frequency domain [2, 11]. Greediness reduces the time-frequency resolution but it can represent an advantage for interception purposes.

2.2 The Chirplet Dictionary

Chirplets are Gaussian-envelope functions with linear frequency modulation. They model many radar signals, especially those coming from low probability of interception radars [16, 17]. Chirplets also exhibit optimum time-frequency concentration [4] (in the sense that they accomplish the generalized uncertainty principle). This leads to time-frequency representations with more physical meaning.

Regarding ISAR imaging, chirplets are often used to represent the echoes from manoeuvring targets or with complex movement [8, 15].

Each chirplet is defined by a 4-parameter vector $\gamma = [\alpha, \beta, T, f]^{\mathrm{T}}$ as follows:

$$h_\gamma(n) = \left(\frac{\alpha}{\pi}\right)^{1/4} e^{-\frac{\alpha}{2}(n-T)^2 + j\left[2\pi f(n-T) + \pi\beta(n-T)^2\right]} . \quad (5)$$

The parameter vector γ has a clear physical meaning: T is the mean time, f is the mean frequency and β is the chirp rate of the linear frequency modulation. α is inversely related to the effective duration of the chirplet, d, according to the expression $d = \sqrt{2/\alpha}$ [3].

2.3 AD Implementations

AD estimates each atom of the expansion by means of an optimization procedure, as shown in Eq. (2). The objective function in this equation can present numerous local maxima and extensive plane regions. For this reason, different AD implementations have been proposed in the literature [5, 6, 11, 18]. The common approach consists of finding out a coarse solution by a global search, and then refining this solution through a local search in a reduced region around the coarse solution. However, the performance of AD is highly dependent on the implementation used, and not all the AD implementations are suitable for ISAR imaging [19].

In this work, we use the implementation referred to as TFAD2 [19]. TFAD2 is an enhanced version of the TFAD algorithm [6, 20] which incorporates several modifications with the aim of improving the TFAD performance for long duration or high chirp rate atoms. TFAD and TFAD2 are efficient methods optimized for chirplet dictionaries, contrary to others AD algorithms (ESAD [5], GAAD [11]) which solve Eq. (2) for any possible dictionary. When using TFAD2, each of the parameters of the chirplet is estimated by maximizing different objective functions.

In our simulations, the input parameters of TFAD2 are: the chirp rate sampling, M_1, is fixed to the number of samples, i.e. the number of successive pulses, and the sampling of α is fixed to $M_2 = 64$. These TFAD2 settings provide an acceptable trade-off between accuracy and computational burden.

3. DENOISING BY AD

3.1 The detection strategy

In order to obtain an ISAR image through AD, the signal expansion of (1) has to be computed for each range cell. For this reason, a stopping criterion is used to avoid long processing times. Thus, the expansion finishes if any of these two conditions are satisfied:

1. 50 atoms has been estimated.
2. The residual signal energy is less than 1 per cent of the input signal energy.

Note that the mere stopping criterion performs a denoising in the ISAR image, unless the signal can be approximated by less than 50 atoms and the energy of all the signal components are greater than 1 per cent of the total signal energy (which is very unlikely when signals are corrupted by noise). Also note that the first condition allows to control the maximum processing time.

However, the effectiveness of the detection strategy (and therefore, its name) is attained when the final expansion, equation 1, is constructed with the extracted atoms which surpass the detection test:

$$\frac{|\widehat{b}_p|^2}{\widehat{\sigma_p}^2} \underset{H_0}{\overset{H_1}{\gtrless}} Th , \quad (6)$$

where the null hypothesis, H_0, is that the signal consists of only noise and the alternate hypothesis, H_1, is that the signal consists of one atom plus noise. $\widehat{b}_p$ is the estimated coefficient of the p-extracted atom, and $\widehat{\sigma_p}^2$ is an estimate of the noise power:

$$\widehat{\sigma_p}^2 = \frac{\|\mathbf{x}_p\|^2}{N} , \quad (7)$$

where N is the number of samples of the signal, $\mathbf{x}$.

The detection test allows to control the false alarm probability for the image. In our case, we set the false alarm probability to $\mathrm{P_{FA}} = 10^{-3}$ for each extracted atom. Once all the atoms are estimated, we use the Adaptive Spectrogram (AS) [3] as the time-frequency (dwell time vs Doppler frequency) representation for each range cell. Finally, all the time-frequency representations are rearranged in order to obtain the sequence of ISAR images through the dwell time [3].

3.2 The classification strategy

This denoising technique is based on the physical meaning of the chirplets parameters. Basically, it consists of separating in the parameter space the noise components from the signal components. Then, when the fluctuation of the target velocity is moderately smooth, chirplets are expected to exhibit low chirp rate magnitude (β). Therefore, atoms with a chirp rate magnitude greater than a given value, are not considered for the signal expansion. Also, the classification strategy is a powerful tool for separating the rotating parts of a target from the main body [15]. In our development, we consider the Doppler range of the target to be unknown, and therefore, the mean frequency of the chirplets cannot be used to discriminate atoms coming from noise. The weak point of this technique is the difficulty to determine an appropriate threshold for the chirp rate, due to non-perfect motion compensation and/or insufficient signal knowledge.

4. RESULTS

4.1 Simulated data

Firstly, we consider the case of a simulated target. The data can be obtained at the web site http://airborne.nrl.navy.mil/∼vchen/data by courtesy of Dr. V.C. Chen of Naval Research Laboratory. The data correspond to a B-727 airplane and have been simulated for a stepped frequency radar operating at 9 GHz and with a bandwidth of 150 MHz. For each pulse, 64 complex range samples were saved. The file contains 256 successive pulses. The Pulse Repetition Frequency (PRF) is 20KHz. Motion compensation and range processing have been applied to the data. However, the fluctuation in velocity has not been compensated. Contrary to an FFT-based ISAR image, AD-based ISAR images are not affected by the target fluctuations in velocity, since chirplets can model these fluctuations. As a reference, the ISAR image obtained by AD is plotted in Figure 1. This image, and all that will be shown, correspond

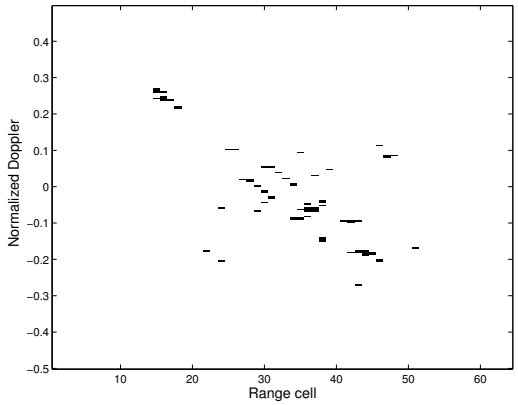

Figure 1: ISAR image for simulated B-727 data and high SNR.

to the 64th pulse within the temporal sequence of ISAR images obtained by AD. The SNR for these data is high, and therefore, the image is not corrupted by noise even when no denoising technique has been used.

In order to evaluate the different denoising strategies, an additive complex white Gaussian noise, with zero mean and variance σ^2, has been added to the data for simulating different SNR. We define the SNR as follows:

$$\mathrm{SNR} = \frac{\sum_{r=1}^{R}\sum_{p=1}^{P}|X(r,p)|^2}{R\,P\,\sigma^2} \tag{8}$$

where R is the number of range samples, P is the number of successive pulses and $X(r,p)$ is the complex data for the r-th range and p-th pulse. The SNR represents the ratio between the mean power of the collected data and the power of the additive noise.

In Figure 2 they are represented the ISAR images obtained by AD with different denoising techniques and for different SNR. In each row, the same denoising technique has been used, and the SNR varies. Thus, the first row corresponds to the case when no denoising technique is used. The second represents the case of using the detection strategy where the probability of false alarm per atom is set to $\mathrm{P_{FA}} = 10^{-3}$. The third row is the same but setting $\mathrm{P_{FA}} = 10^{-1}$. Finally, the last row corresponds to the case when the classification strategy is used (chirp rate discrimination) in combination with the AD detector ($\mathrm{P_{FA}} = 10^{-1}$). In each column, the images correspond to the same SNR and different denoising techniques.

As can be seen, for SNR=0 dB (first column), the images obtained has been nearly not corrupted by noise, even when no denoising technique has been used. However, for lower SNR it is necessary to use a denoising strategy since otherwise the images are highly corrupted by noise. In the second row, the detection strategy is very effective for all the SNR considered when $\mathrm{P_{FA}} = 10^{-3}$, and no false alarms can be seen in the images. However, some signal components are missed as the SNR decreases, and only the most powerful components can be appreciated for SNR$= -10$ dB. In the third row, when only the detection technique is used but setting $\mathrm{P_{FA}} = 10^{-1}$, there is many more false alarms than for $\mathrm{P_{FA}} = 10^{-3}$. On the other hand, a lesser number of signal components are missed when $\mathrm{P_{FA}} = 10^{-1}$. Thus, the aim of using the classification strategy in combination with the detector is to clean the ISAR image from the false alarms obtained with a high $\mathrm{P_{FA}}$ while keeping the weak signal components in the image. This objective is only attained in part since although all the signal components are preserved, not all the false alarms has been wiped out.

Finally, it has been said that the classification strategy separates signal components from noise components by using the chirp rate parameter. Figure 3 serves to explain the motivation of this strategy. In continuous trace, it is plotted the simulated probability density function (100.000 trials) of the chirp rate magnitude of chirplets estimated by AD when there is only noise at the input. The dashed line corresponds to the histogram of the chirp rate magnitude for the B-727 simulated data, in the absence of additive noise. It can be appreciated that all the signal components exhibit a chirp rate magnitude lesser than the value $2 \cdot 10^{-3}$ (marked with a dotted vertical trace), which is the threshold used by the classification technique in Figure 2 and allows to clean the image from all the noise components exhibiting a greater chirp rate magnitude. Note that the probability of false alarm will depend on the target and its movement.

5. REAL LIFE DATA

The purpose of this section is to evaluate the AD-based denoising techniques for real life data. In this case, 128 complex range samples were saved for each pulse and the data comprises 128 successive pulses. The rest of parameters remain equal to the previous case.

Figure 4 shows the ISAR images obtained by AD for these real data, when no denoising technique is used (a) and when the detector is used with $\mathrm{P_{FA}} = 10^{-3}$. It can be seen that the SNR is relatively high, since the number of false alarms in the image obtained with no denoising is small. As with simulated data, it can be seen that the use of the detector cleans the image from false alarms near completely. In case of using the FFT to obtain the ISAR image Figure 4(c), the noise covers the whole image and the use of a threshold is mandatory. For instance, the image can be represented by using a color scale for the image intensity. In our case, we have represented in Figure 4(d) only the image points exceeding a given threshold. This threshold is set to attain a $\mathrm{P_{FA}} = 10^{-3}$ per pixel (contrary to AD, where the $\mathrm{P_{FA}}$ is defined per atom). It is noteworthy that the analysis of the sequence of images obtained by AD shows that the fluctuations in velocity are negligible (the chirp rate of the atoms is near zero). In such a case (complete movement compensation), the FFT is the best processing algorithm since it becomes the matched filter of the signal echoes.

6. CONCLUSION

AD has an increasing use in areas such as signal detection and radar image processing (ISAR). We proposed to use AD not only as an algorithm to generate the ISAR image but also as a processing tool to improve the quality of the image by denoising. Different denoising techniques has been proposed, resulting the use of a detector as the most suitable a priori since it allows to fix the probability of false alarm per atom and does not require a previous knowledge of the signal.

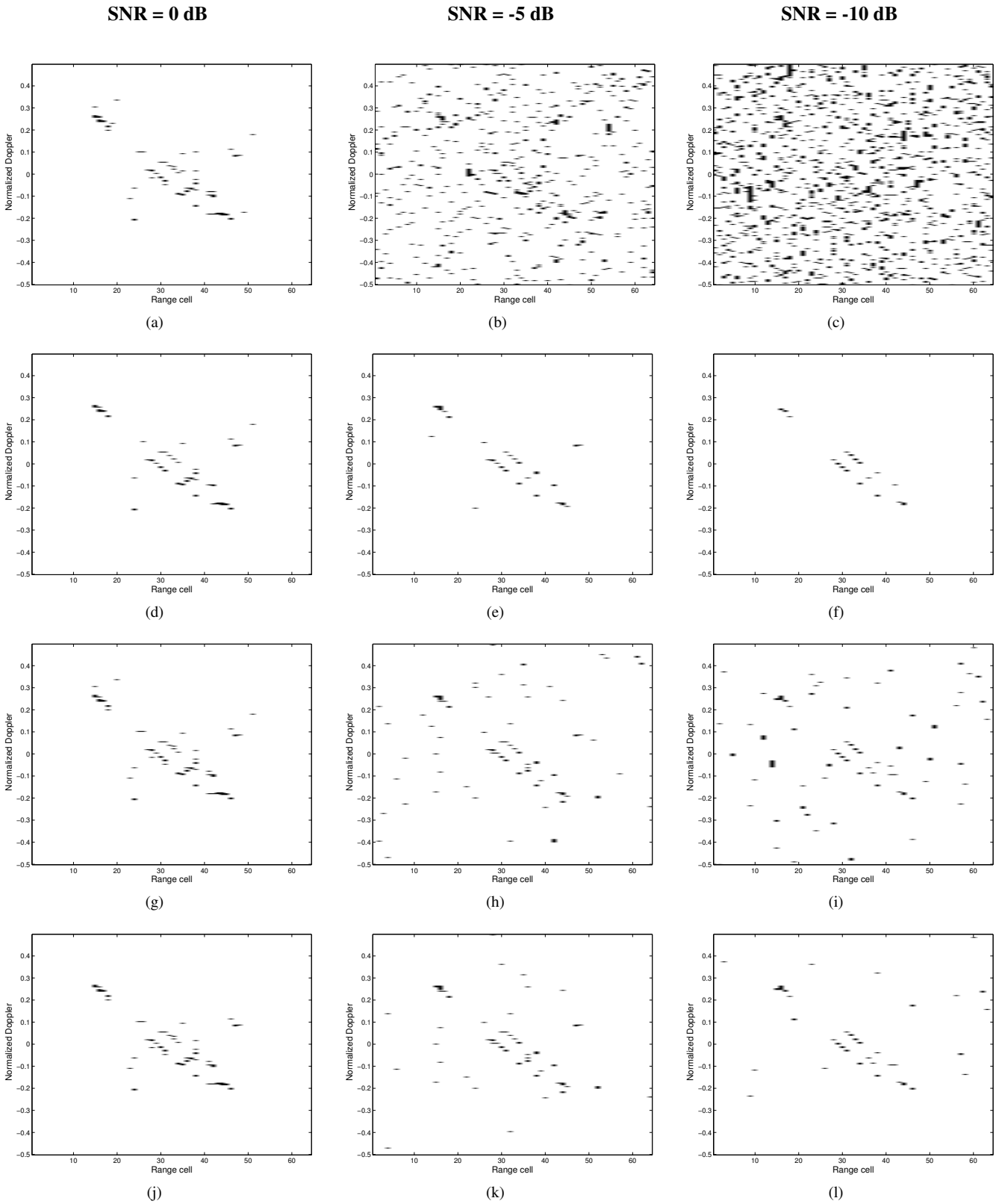

Figure 2: ISAR images for simulated B-727 data. SNR indicated at the top. (a)-(c) No denoising. (d)-(f) Detector is used with $P_{FA} = 10^{-3}$. (g)-(i) Detector is used with $P_{FA} = 10^{-1}$. (j)-(l) Detector is used with $P_{FA} = 10^{-1}$ and classification using the chirp rate.

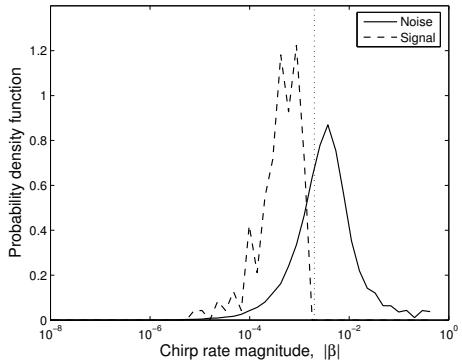

Figure 3: Representation of the chirp rate classifier.

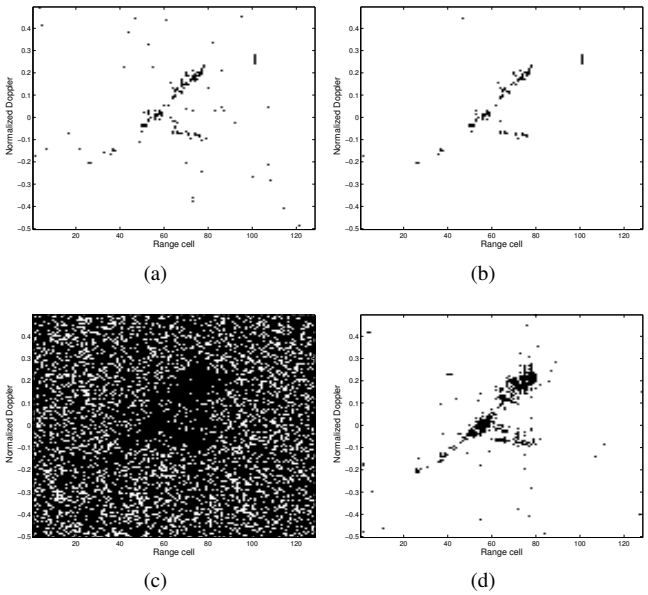

Figure 4: ISAR images for real B-727 data. (a) AD with no denoising. (b) AD using the detector and $P_{FA} = 10^{-3}$. (c) FFT with no detector. (d) FFT using a threshold to attain $P_{FA} = 10^{-3}$.

7. ACKNOWLEDGEMENTS

This work was supported by Project TEC2005-07010-C02-01/TCM of the National Board of Scientific and Technological Research (CICYT). The authors also wish to thank Dr. Victor .C. Chen of Naval Research Laboratory for providing the measurement data used in this work.

REFERENCES

[1] F. Hlawatsch and G. F. Boudreaux-Bartels, "Linear and Quadratic Time-Frequency Signal Representations," *IEEE Signal Processing Magazine*, pp. 21–67, April 1992.

[2] S. Mallat, *A Wavelet Tour of Signal Processing*, Academic Press, 1998.

[3] S. Qian and D. Chen, *Joint Time-Frequency Analysis. Methods and Applications*, Prentice Hall, 1996.

[4] L. Cohen, *Time-Frequency Analysis*, Prentice Hall, 1995.

[5] A. Bultan, "A four-parameter atomic decomposition of chirplets," *IEEE T-SP*, vol. 47, no. 3, pp. 731–745, March 1999.

[6] J. C. O'Neill and P. Flandrin, "Chirp hunting," in *IEEE TFTS*, 1998, pp. 425–428.

[7] S. G. Mallat and Z. Zhang, "Matching pursuits with time-frequency dictionaries," *IEEE T-SP*, vol. 41, no. 12, pp. 3397–3415, Dec. 1993.

[8] G. Wang, X.-G. Xia, B.T. Root, V.C. Chen, Y. Zhang, and M. Amin, "Manoeuvering target detection in over-the-horizon radar using adaptive clutter rejection and adaptive chirplet transform," *IEE Proc.- Radar, Sonar and Nav.*, vol. 150, no. 4, pp. 292–298, August 2003.

[9] T. Thayaparan, G. Lampropoulos, S.K. Wong, and E. Riseborough, "Application of adaptive joint time-frequency algorithm for focusing distorted ISAR images from simulated and measured radar data," *IEE Proc.- Radar, Sonar and Nav.*, vol. 150, no. 4, pp. 213–220, August 2003.

[10] I.-S. Choi, B.-L. Cho, and H.-T. Kim, "ISAR motion compensation using evolutionary adaptive wavelet transform," *IEE Proc.- Radar, Sonar and Nav.*, vol. 150, no. 4, pp. 229–233, August 2003.

[11] G. López-Risueño, J. Grajal, and O. Yeste-Ojeda, "Atomic decomposition-based radar complex Signal interception," *IEE Proc.-Radar, Sonar and Nav.*, vol. 150, pp. 323–331, August 2003.

[12] G. López-Risueño and J. Grajal, "Multiple signal detection and estimation using atomic decomposition and expectation maximization," *IEEE Trans. on Aerospace and Electronic Systems*, vol. 42, no. 1, January 2006.

[13] V.C. Chen and Hao Ling, *Time-Frequency Transforms for Radar Imaging and Signal Analysis*, Artech House, 2002.

[14] L.C. Trintinalia and H. Ling, "Joint time-frequency ISAR using adaptive processing," *IEEE Trans. on Antennas and Propagation*, vol. 45, no. 2, pp. 221–227, Feb. 1997.

[15] J. Li and H. Ling, "Application of adaptive chirplet representation for ISAR feature extraction from targets with rotating parts," *IEE Proc.- Radar, Sonar and Nav.*, vol. 150, no. 4, pp. 284–291, August 2003.

[16] P. H. Pace, *Detecting and Classifying Low Probability of Intercept Radar*, Artech House, 2004.

[17] M. Perez, A. Asensio, J. Gismero, J. I. Alonso, J.M. Monje, F. Casanova, R. Cortijo, and J. F. Perez-Ojeda, "Aries: a high-resolution shipboard radar," in *Proc. of IEEE Radar Conference*, 2002, pp. 148–153.

[18] Q. Yin, S. Qian, and F. Aigang, "A fast refinement for adaptive gaussian chirplet decomposition," *IEEE T-SP*, vol. 50, no. 6, pp. 1298–1306, June 2002.

[19] O. Yeste-Ojeda, J. Grajal, and G. López-Risueño, "Atomic decomposition for radar applications," Submitted to IEEE Trans. on Aerospace and Electronic Systems.

[20] J. C. O'Neill, P. Flandrin, and W. C. Karl, "Sparse representation with chirplets via maximum likelihood estimation," 2000, Paper available at http://tfd.sourceforge.net/Papers/chirp.pdf.

[21] G. Zweig, "Super-resolution fourier transforms by optimisation, and ISAR imaging," *IEE Proc.- Radar, Sonar and Nav.*, vol. 150, no. 4, pp. 247–252, August 2003.